JACS
JOURNAL OF THE AMERICAN CHEMICAL SOCIETY

Article

pubs.acs.org/JACS

Simulative and Experimental Characterization of a pH-Dependent Clamp-like DNA Triple-Helix Nanoswitch

Federico Iacovelli,[†,#] Andrea Idili,[‡,#] Alessandro Benincasa,[†] Davide Mariottini,[‡] Alessio Ottaviani,[†] Mattia Falconi,[†] Francesco Ricci,*[,‡] and Alessandro Desideri*[,†]

[†]Department of Biology and [‡]Department of Chemistry, University of Rome, Tor Vergata, 00173 Rome, Italy

Supporting Information

ABSTRACT: Here we couple experimental and simulative techniques to characterize the structural/dynamical behavior of a pH-triggered switching mechanism based on the formation of a parallel DNA triple helix. Fluorescent data demonstrate the ability of this structure to reversibly switch between two states upon pH changes. Two accelerated, half microsecond, MD simulations of the system having protonated or unprotonated cytosines, mimicking the pH 5.0 and 8.0 conditions, highlight the importance of the Hoogsteen interactions in stabilizing the system, finely depicting the time-dependent disruption of the hydrogen bond network. Urea-unfolding experiments and MM/GBSA calculations converge in indicating a stabilization energy at pH 5.0, 2-fold higher than that observed at pH 8.0. These results validate the pH-controlled behavior of the designed structure and suggest that simulative approaches can be successfully coupled with experimental data to characterize responsive DNA-based nanodevices.

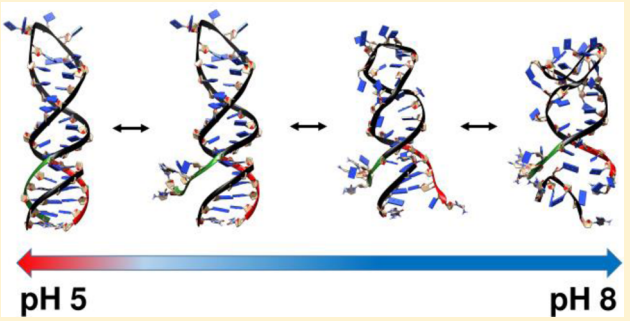

INTRODUCTION

DNA nanotechnology allows us to design and engineer smart nanomaterials and nanodevices using synthetic DNA sequences.[1−6] For example, current methodologies and synthetic strategies, such as DNA tiles, origami, or supramolecular assembly, allowed the production of complex nanostructures of different shapes and dimensions.[7−11] The unparalleled versatility of these approaches allows precise positioning of molecule-responsive switching elements in specific locations of DNA nanostructures, leading to the construction of more complex functional nanodevices.[12−14] Similarly, enzyme−DNA nanostructures have been demonstrated to enhance enzyme catalytic activity and stability.[15] DNA motifs that rely on noncanonical DNA interactions, such as G-quadruplex, triplex, i-motif, hairpin, and aptamers, can be used to design such nanodevices due to their dynamic-responsive behavior toward chemical and environmental stimuli.[16,17] These responsive units often respond to specific chemical inputs through a binding-induced conformational change mechanism that leads to a measurable output or function. The efficiency of this class of responsive nanodevices strongly depends on the designed structure-switching mechanism that controls their activity or functionality. Therefore, there is an urgent need to understand the energies involved in these responsive systems and the relationship between their structure and dynamics.[16]

Among such functional DNA nanodevices, those based on the triple-helix motif are attracting interest for their strong and programmable pH dependence.[18−20] By rationally incorporating triplex-forming portions into DNA nanodevices, it is possible to trigger conformational changes and functions using pH as a chemical input.[21−24] Despite the fair amount of knowledge of the basic design principles and mechanism of action of triplex-based nanodevices, no reports describing the connection between their structural and dynamical properties are available. Toward this aim, simulative approaches represent valuable tools to shed light on the structural, thermodynamic and dynamic properties of DNA nanostructures.[14,25−30] The synergy between experiments and molecular dynamics (MD) simulations may provide significant information for the rational design of functional, pH-activated nanodevices based on a triple-helix motif.

Motivated by the above arguments, here we demonstrate how a combined simulative/experimental approach can be exploited to provide an atomistic description of DNA-based structure-switching mechanisms. As test bed for this study, we have focused on the structural/dynamical behavior of a well-characterized pH-triggered switching mechanism based on the formation of a parallel DNA triple helix[31−35] through a simple two-state clamp-like switching mechanism (Figure 1). The flexibility and modularity of this mechanism permits the fine tuning of the reactivity of different nanomaterials and nanodevices toward pH as demonstrated in recent works.[3,23,24,36] The computational and experimental data presented here indicate that the system is able to form a stable triple helix at pH 5.0, while at pH 8.0 there is no presence of

Received: November 4, 2016
Published: April 2, 2017

DOI: 10.1021/jacs.6b11470
J. Am. Chem. Soc. XXXX, XXX, XXX−XXX

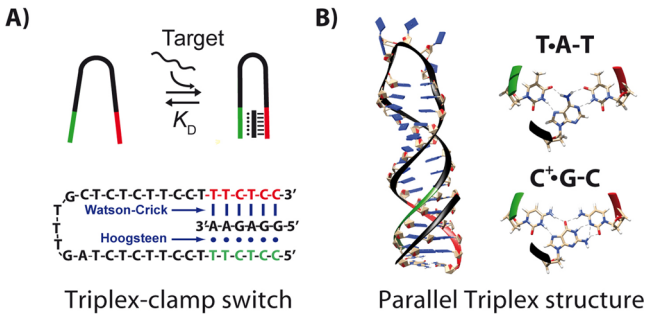

Figure 1. Clamp-like triplex forming DNA nanoswitch here used as a model system: (A) The DNA clamp-like receptor is designed to have a duplex-forming portion (red in the figure) that recognizes through WC interactions a 6-base specific DNA sequence. Such first recognition element is linked, through a random loop (black), to a triplex-forming portion (green) able to recognize the double-stranded DNA and to form a triplex structure composed of both WC and parallel Hoogsteen interactions. (B) Molecular view of the triple-helix structure generated through the formation of the TAT and C^+GC triplets between the clamp-switch and its complementary 6-base DNA strand. C^+GC triplets require the protonation of the N3 of cytosine in the third strand (green) that are therefore stable only at acid pHs (average pK_a of protonated cytosines in triplex structure is ~6.5).[18] On the contrary, TAT triplets are stable at neutral pH and can unfold at higher pHs due to deprotonation of thymine ($pK_a \approx 10$).[20]

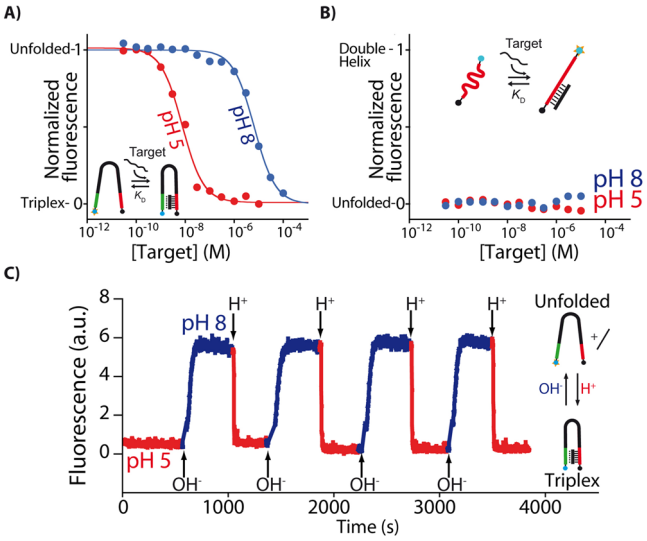

Figure 2. Triplex clamp-switch shows a strong pH-dependent behavior. (A) The affinity of the triplex clamp-switch for its complementary 6-base DNA target is higher at pH 5.0 (red curve) than at pH 8.0 (blue curve). (B) The control linear probe that retains the same WC recognition element of the triplex clamp-switch but lacks the triplex-forming portion is not able to bind the complementary 6-base DNA strand in the same specific target concentration window and at both pHs (red and blue curves). (C) By cyclically changing the pH of a solution containing the triplex clamp-switch and its complementary target from 5.0 to 8.0 we can follow the reversible behavior of the switching mechanism. Here, the binding curves were obtained by adding increasing concentration of a 6-base DNA target to a 10 nM concentration of clamp-switch (A) or control linear (B) in 40 mM Tris buffer, 12.6 mM $MgCl_2$ at the indicated pHs and at 25 °C. For the pH-cycle experiment the solution contains the clamp-switch (10 nM) with the 6-base DNA target (1 μM), and the pH of the solution was cyclically changed by adding small aliquots of 3 M NaOH or HCl in 40 mM Tris buffer, 12.6 mM $MgCl_2$ at 25 °C.

the triple- and even of the double-helical structures. Two accelerated MD (aMD) simulations[37] (500 ns each) of the system, having protonated or unprotonated cytosines mimicking the pH 5.0 and 8.0 conditions, unravelled the atomistic detail of the folded to unfolded transition characterizing the two-state switching mechanism. The present study sets the basis for combined use of experimental and computational approaches to understand the mechanism of novel and efficient nanodevices to be included in complex nanosystems.

EXPERIMENTAL SECTION

Reagents and Materials. All chemicals, including Trizma base (tris(hydroxymethyl)aminomethane), magnesium chloride, hydrochloric acid, sodium hydroxide, and ultrapure urea, were of analytical grade and were purchased from Sigma-Aldrich (St. Louis, MO) unless otherwise indicated.

Oligonucleotides. All oligonucleotide employed in this work were synthesized, labeled, and purified (HPLC and reverse phase) by IBA GmBH (Göttingen, Germany) and used without further purification. Unless otherwise stated, the labeled oligonucleotides were dissolved in Millipore water at a concentration of 1 mM, while the nonlabeled oligonucleotides were dissolved in the relevant buffer (40 mM Tris buffer, 12.6 mM $MgCl_2$, pH 5.0 and 8.0) at a concentration of 100 μM. The final concentration of the oligonucleotides was confirmed using Tecan Infinite M200pro (Männedorf, Switzerland) through a NanoQuant Plate. Before use, each labeled oligonucleotide solution was heated to 95 °C for 5 min and then allowed to cool to room temperature for 2 h. We used a triplex clamp-switch and a linear probe bearing the same recognition element of six bases. These are labeled with Alexafluor 680 (AF680) and Black Hole Quencher 2 (BHQ-2) at the 5′ and 3′ ends. The sequences of the probes were as follows:

Triplex clamp-switch: 5′-*CCTTT*-TCCTTCTCTCGTTTGCTC-TCTTCCT-**TTCTCC**-3′

Linear probe: 5′-CTCTCTTCCT-**TTCTCC**-3′

For the above sequences, the bases in bold represent the duplex-forming portion (red portion in Figures 1 and 2). In the clamp-switch, the underlined bases represent the random loop sequence (black portion in Figures 1 and 2), and the italic bases represent the triplex-forming portion (green portion in Figures 1 and 2). The structure-switching mechanisms of the two probes used in this work are depicted in Figures 1 and 2. Perfect match target was also synthesized and HPLC purified from IBA GmBH (Göttingen, Germany). The sequence of the complementary homopurine 6-base DNA strand was as follows:

Target (6 bases): 5′-GGAGAA-3′

We have also used additional clamp-switches to demonstrate the effect of nonspecific interactions in the kinetic folding and unfolding and to better highlight the role of simulative data. These switches are also labeled with Alexafluor 680 (AF680) and Black Hole Quencher 2 (BHQ-2) at the 5′ and 3′ ends and have the following sequences:

5-base loop triplex clamp-switch: 5′-*CCTCTT*-GTTTG-**TTC-TCC**-3′

12-base target triplex clamp-switch: 5′-*CCTCTTTCCTTC* GTTTG **CTTCCTTTCTCC**-3′

For these sequences, the bases in bold represent the duplex-forming portion, the underlined bases represent the random loop sequence, and the italic bases represent the triplex-forming portion. The perfect match 12-base DNA strand sequence is as follows:

Target (12 bases): 5′-GGAGAAAGGAAG-3′

Binding Curves. All binding curve experiments were obtained using a fixed concentration of the triplex clamp-switch or linear probe (10 nM) and by adding increasing concentrations of a stock solution of the 6-base or 12-base DNA target in a 800 μL volume cuvette. The experiments were conducted in 40 mM Tris buffer, 12.6 mM $MgCl_2$ at different pHs at 25 °C. The fluorescence measurements were obtained using a Cary Eclipse Fluorimeter with excitation at 679 (±5) nm and acquisition between 690 and 712 nm. The fluorescence signals at each target concentration were recorded every 10 min until they reached

DOI: 10.1021/jacs.6b11470
J. Am. Chem. Soc. XXXX, XXX, XXX−XXX

equilibrium. The equilibrated values were fitted to a single-site binding mechanism ([X] = target concentration; F_B = fluorescence in the presence of saturating concentration of target; $F_{[T]}$ = fluorescence in the presence of different concentrations of target; F_0 = background fluorescence):

$$F_{[T]} = F_0 + \left(\frac{[X](F_B - F_0)}{[X] + K_D} \right)$$

Kinetic Fluorescence Experiment. The kinetic experiment was performed using a fixed concentration of the triplex clamp-switch (10 nM) in the presence of a saturated amount of 6-base DNA target (1 μM) and at pH 5.0 in a 1400 μL volume stirred cuvette, monitoring the fluorescence signal corresponding to the clamp-switch in the folded triplex state. Successively, the pH of the solution was cyclically changed between pH 8.0 and 5.0 by addition of small aliquots of 3 M NaOH or HCl.

Urea Titration Curve Experiments. Urea titration curves of the triplex clamp-switch in the presence of the DNA complementary target were obtained by sequentially increasing the urea concentration of the buffer solution (40 mM Tris buffer, 12.6 mM $MgCl_2$, pH 5.0 and 8.0) containing the labeled clamp-switch (10 nM) and a saturated amount of the complementary 6-base DNA strand (30 μM) from 0 to 9.5 M. This was achieved by removing small volume of the sample prepared in the working buffer solution and replacing it with a similar volume of clamp-switch (10 nM) and a saturated amount of the complementary 6-base target (30 μM) dissolved in 10 M urea solution and prepared with the same buffer salts (40 mM Tris buffer, 12.6 mM $MgCl_2$, pH 5.0 and 8.0). For each urea concentration, the system was allowed to equilibrate for 3 min prior to measurement. The fluorescence measurements were obtained using a Cary Eclipse fluorimeter with excitation at 679 (±5) nm and acquisition between 690 and 712 nm at a temperature of 25 °C. The fluorescence value at 702 nm (corresponding to the maximum emission of AF680) was used to build the urea titration curves. We determined binding free energies between the clamp-switch and the target strand (at pH 5.0 and 8.0) by fitting the urea titration curves (fluorescence (F) versus urea concentration, [U]) using a two-state unfolding model (see the SI for details)[31,38,39]

$$F = \frac{[T_{tot}](F^{\circ}_F + \sigma_F[U]) + (F^{\circ}_{UN} + \sigma_{UN}[U])e^{-(\Delta G^{\circ}_B(H_2O) - m[U])/RT}}{([T_{tot}] + e^{-(\Delta G^{\circ}_B(H_2O) - m[U])/RT})}$$

where $\Delta G^{\circ}_B(H_2O)$ is the binding free energy, m is the dependence of $\Delta G^{\circ}_B(H_2O)$ on urea concentration (kcal/M·mol), F°_F and F°_{UN} are the fluorescence signals of the folded (bound) and unfolded (unbound) states, respectively, in absence of urea, and σ_F and σ_{UN} represent the dependence of the fluorescence signal of the folded and unfolded states, respectively, on urea concentration. To improve the precision of the fit for the urea titration curve of the clamp-switch in the presence of the DNA target at pH 8.0, we fixed the σ_F value, the dependence of the fluorescence signal of the bound state (triplex state) on urea concentration using the value obtained by linear extrapolation of the initial portion of the curve obtained at pH 5.0 (0.2983 M^{-1}).[31,38,39] While for the urea titration curve of the clamp-switch in the presence of the DNA target at pH 5.0 we fixed the σ_{UN} value, the dependence of the fluorescence signal of the unbound state (unfolded state) on urea concentration using the value obtained by linear extrapolation of the final portion of the curve obtained at pH 8.0 (0.5243 M^{-1}).[31,38,39]

Molecular Dynamics Simulations. The fiber module of the X3DNA program[40] has been used to generate the PDB file template of the triple-helix model, exclusively formed by TAT sequence repetitions. The nucleotide sequence of the strands composing the triple helix has been modified through the X3DNA mutate_bases module[40] in order to match the designed oligonucleotides sequences. The Watson–Crick (WC) strand has been connected to the triplex-forming strand through the sculpting module of the PyMol program[41] to generate the triplex clamp-switch final structure (Figure 1). The structure has been minimized using the UCSF Chimera program[42] to remove any clashes and unwanted interactions introduced by the strands connection modeling. The system topologies and the coordinates of the triple helix at the two pH conditions (i.e., pH 5.0 and 8.0), used as input for the AMBER 14 MD package,[43] have been obtained through the AmberTools tLeap module, parametrizing the structures through the AMBER ff14SB force field[44] with the parmbsc1 corrections.[45] To simulate the pH 5.0 conditions, the residue names of cytosines, composing the triplex-forming strand, were changed according to the AMBER nomenclature for protonated nucleotides. The structures were immersed in a rectangular box filled with TIP3P water molecules,[46] imposing a minimum distance between the solute and the box of 14 Å, and the charges were neutralized adding Mg^{2+} counterions to the solvated systems in favorable positions, as implemented in the tLeap program.[43] For each structure, a minimization run was performed for 2500 steps using the steepest descent algorithm, imposing a harmonic constraint of 50 kcal·mol^{-1}·Å^{-2}, to remove any unfavorable interaction and to prevent irreversible Mg^{2+} binding to DNA. The systems were gradually heated from 0 to 300 K in the NVT ensemble over a period of 500 ps using the Langevin thermostat,[47] with a coupling coefficient of 1.0 ps and a weak constraint of 15 kcal·mol^{-1}·Å^{-2} on nucleotides. At the end of the equilibration phase, the systems were subjected to an equilibrium simulation for 500 ps to remove all constraints. The optimized systems were then simulated using the isobaric–isothermal ensemble (NPT) for 10 ns, using periodic boundary conditions, and a 2.0 fs time-step, using the PME method[48] for the long-range electrostatic interactions with a cutoff of 9 Å for the evaluation of short-range nonbonded interactions. The SHAKE algorithm[49] was used to constrain covalent bonds involving hydrogen atoms. The temperature was fixed at 313 K using the Langevin dynamics,[47] while pressure was held constant at 1 atm through the Langevin piston method.[50] Atomic positions were saved every 500 steps (1.0 ps) for the analyses.

Accelerated Molecular Dynamics Simulations. The classical MD simulations have been carried out to extract the average potential and the average dihedral energies, required by the aMD technique,[37] to modify the potential energy landscape. The aMD technique permits, due to the introduction of a bias potential, access to a large conformational space that cannot be normally accessed by classical MD. The potential modification reduces the local barrier height and allows the calculation to evolve much faster. aMD only requires the evolution of a single copy of the system and does not require any previous knowledge of the potential shape. Each system has been simulated for 500 ns. All simulations were entirely performed using an NVIDIA Tesla K40C GPU.

Trajectory Analysis. Root-mean-square deviations (RMSDs), hydrogen bond time evolution, and PCA analyses have been carried out over the entire 500 ns trajectories by using the GROMACS 4.6.7 analysis tools.[51,52] The hydrogen bond number was evaluated, through the g_hbond module, using an angle cutoff of 30° and a donor–acceptor distance of 3.5 Å. MM-GBSA calculations were performed using the MMPBSA.py code included in the AmberTools distribution.[53] The solvent accessible surfaces were calculated through the CPPTRAJ tool of the AmberTools distribution,[54] while the buried surface areas (BSA) were computed by the formula:

$$BSA = \frac{SAS_{system} - SAS_{clamp\text{-}switch} - SAS_{target}}{2}$$

The reweight of aMD trajectories to recover canonical ensemble and the original free energy profile of the simulated structures has been executed using PyReweighting,[55] a toolkit of python scripts to facilitate the aMD simulation reweighting.

RESULTS AND DISCUSSION

Fluorescence Experiments. The clamp-switch triplex-forming DNA sequence employed here is a 37 base long oligonucleotide comprising two recognition elements of 6 bases (Figure 1, red and green), separated by a loop of 25 bases (Figure 1, black). The switch is labeled with a fluorophore

DOI: 10.1021/jacs.6b11470
J. Am. Chem. Soc. XXXX, XXX, XXX–XXX

■ ASSOCIATED CONTENT

Supporting Information

The Supporting Information is available free of charge on the ACS Publications website at DOI: 10.1021/jacs.6b11470.

Urea fitting equation and supplementary figures (PDF)

■ AUTHOR INFORMATION

Corresponding Authors

*francesco.ricci@uniroma2.it
*desideri@uniroma2.it

ORCID

Andrea Idili: 0000-0002-6004-270X
Francesco Ricci: 0000-0003-4941-8646

Author Contributions

#F.I. and A.I. contributed equally.

Notes

The authors declare no competing financial interest.

■ ACKNOWLEDGMENTS

This work was supported by Associazione Italiana per la Ricerca sul Cancro, AIRC (Project No. 14420) (FR), by the European Research Council, ERC (Project No. 336493) (FR), by the Italian Ministry of University and Research (Project of National Interest, PRIN, 2012 CTAYSY), and by the NVIDIA Corporation (donation of Tesla K40C to M.F.).

■ REFERENCES

(1) Um, S. H.; Lee, J. B.; Park, N.; Kwon, S. Y.; Umbach, C. C.; Luo, D. *Nat. Mater.* **2006**, *5*, 797.
(2) Kuzyk, A.; Schreiber, R.; Fan, Z.; Pardatscher, G.; Roller, E.-M.; Högele, A.; Simmel, F. C.; Govorov, A. O.; Liedl, T. *Nature* **2012**, *483*, 311.
(3) Huang, F.; Liao, W. C.; Sohn, Y. S.; Nechushtai, R.; Lu, C. H.; Willner, I. *J. Am. Chem. Soc.* **2016**, *138*, 8936.
(4) Liu, W.; Halverson, J.; Tian, Y.; Tkachenko, A. V.; Gang, O. *Nat. Chem.* **2016**, *8*, 867.
(5) Ke, Y.; Meyer, T.; Shih, W. M.; Bellot, G. *Nat. Commun.* **2016**, *7*, 10935.
(6) Langecker, M.; Arnaut, V.; Martin, T. G.; List, J.; Renner, S.; Mayer, M.; Dietz, H.; Simmel, F. C. *Science* **2012**, *338*, 932.
(7) Winfree, E.; Liu, F.; Wenzler, L. A.; Seeman, N. C. *Nature* **1998**, *394*, 539.
(8) Wei, B.; Dai, M.; Yin, P. *Nature* **2012**, *485*, 623.
(9) Rothemund, P. W. K. *Nature* **2006**, *440*, 297.
(10) Douglas, S. M.; Marblestone, A. H.; Teerapittayanon, S.; Vazquez, A.; Church, G. M.; Shih, W. M. *Nucleic Acids Res.* **2009**, *37*, 5001.
(11) McLaughlin, C. K.; Hamblin, G. D.; Aldaye, F. a; Yang, H.; Sleiman, H. F. *Chem. Commun.* **2011**, *47*, 8925.
(12) Andersen, E. S.; Dong, M.; Nielsen, M. M.; Jahn, K.; Subramani, R.; Mamdouh, W.; Golas, M. M.; Sander, B.; Stark, H.; Oliveira, C. L. P.; Pedersen, J. S.; Birkedal, V.; Besenbacher, F.; Gothelf, K. V.; Kjems, J. *Nature* **2009**, *459*, 73.
(13) Douglas, S. M.; Bachelet, I.; Church, G. M. *Science* **2012**, *335*, 831.
(14) (a) Juul, S.; Iacovelli, F.; Falconi, M.; Kragh, S. L.; Christensen, B.; Frøhlich, R.; Franch, O.; Kristoffersen, E. L.; Stougaard, M.; Leong, K. W.; Ho, Y. P.; Sørensen, E. S.; Birkedal, V.; Desideri, A.; Knudsen, B. R. *ACS Nano* **2013**, *7*, 9724. (b) Franch, O.; Iacovelli, F.; Falconi, M.; Juul, S.; Ottaviani, A.; Benvenuti, C.; Biocca, S.; Ho, Y.-P.; Knudsen, B. R.; Desideri, A. *Nanoscale* **2016**, *8*, 13333.
(15) (a) Zhao, Z.; Fu, J.; Dhakal, S.; Johnson-Buck, A.; Liu, M.; Zhang, T.; Woodbury, N. W.; Liu, Y.; Walter, N. G.; Yan, H. *Nat. Commun.* **2016**, *7*, 10619. (b) Gao, Y.; Roberts, C. C.; Toop, A.; Chang, C. A.; Wheeldon, I. *ChemBioChem* **2016**, *17*, 1430−1436.
(16) Yatsunyk, L. A.; Mendoza, O.; Mergny, J. L. *Acc. Chem. Res.* **2014**, *47*, 1836.
(17) Wang, F.; Liu, X.; Willner, I. *Angew. Chem., Int. Ed.* **2015**, *54*, 1098.
(18) Leitner, D.; Schröder, W.; Weisz, K. *Biochemistry* **2000**, *39*, 5886.
(19) Sugimoto, N.; Wu, P.; Hara, H.; Kawamoto, Y. *Biochemistry* **2001**, *40*, 9396.
(20) Idili, A.; Vallée-Bélisle, A.; Ricci, F. *J. Am. Chem. Soc.* **2014**, *136*, 5836.
(21) Chen, Y.; Lee, S. H.; Mao, C. *Angew. Chem., Int. Ed.* **2004**, *43*, 5335.
(22) Han, X.; Zhou, Z.; Yang, F.; Deng, Z. *J. Am. Chem. Soc.* **2008**, *130*, 14414.
(23) Porchetta, A.; Idili, A.; Vallée-Bélisle, A.; Ricci, F. *Nano Lett.* **2015**, *15*, 4467.
(24) Idili, A.; Porchetta, A.; Amodio, A.; Vallée-Bélisle, A.; Ricci, F. *Nano Lett.* **2015**, *15*, 5539.
(25) Yoo, J.; Aksimentiev, A. *Proc. Natl. Acad. Sci. U. S. A.* **2013**, *110*, 20099.
(26) Yoo, J.; Aksimentiev, A. *J. Phys. Chem. Lett.* **2015**, *6*, 4680.
(27) Maffeo, C.; Yoo, J.; Aksimentiev, A. *Nucleic Acids Res.* **2016**, *44*, 3013.
(28) Iacovelli, F.; Alves, C.; Falconi, M.; Oteri, F.; De Oliveira, C. L. P.; Desideri, A. *Biopolymers* **2014**, *101*, 992.
(29) Alves, C.; Iacovelli, F.; Falconi, M.; Cardamone, F.; Morozzo Della Rocca, B.; De Oliveira, C. L. P.; Desideri, A. *J. Chem. Inf. Model.* **2016**, *56*, 941.
(30) Iacovelli, F.; Falconi, M.; Knudsen, B. R.; Desideri, A. *RSC Adv.* **2016**, *6*, 35160.
(31) Idili, A.; Plaxco, K. W.; Vallée-Bélisle, A.; Ricci, F. *ACS Nano* **2013**, *7*, 10863.
(32) Kandimalla, E. R.; Agrawal, S. *Gene* **1994**, *149*, 115.
(33) Kandimalla, E. R.; Manning, A.; Agrawal, S. *J. Biomol. Struct. Dyn.* **1996**, *14*, 79.
(34) Xodo, L. E.; Manzini, G.; Quadrifoglio, F. *Nucleic Acids Res.* **1990**, *18*, 3557.
(35) Frank-Kamenetskii, M. D.; Mirkin, S. M. *Annu. Rev. Biochem.* **1995**, *64*, 65.
(36) Lv, Y.; Hao, L.; Hu, W.; Ran, Y.; Bai, Y.; Zhang, L. *Sci. Rep.* **2016**, *6*, 29321.
(37) Hamelberg, D.; Mongan, J.; McCammon, J. A. *J. Chem. Phys.* **2004**, *120*, 11919.
(38) Santoro, M. M.; Bolen, D. W. *Biochemistry* **1988**, *27*, 8063.
(39) Myers, J. K. K.; Pace, C. N. N.; Scholtz, J. M. M. *Protein Sci.* **1995**, *4*, 2138.
(40) Lu, X. J.; Olson, W. K. *Nucleic Acids Res.* **2003**, *31*, 5108.
(41) DeLano, W. L. *PyMOL*; Schrödinger LLC, 2002, http://www.pymol.org, accessed January 20, 2017.
(42) Pettersen, E. F.; Goddard, T. D.; Huang, C. C.; Couch, G. S.; Greenblatt, D. M.; Meng, E. C.; Ferrin, T. E. *J. Comput. Chem.* **2004**, *25*, 1605.
(43) Salomon-Ferrer, R.; Case, D. A.; Walker, R. C. *Wiley Interdiscip. Rev. Comput. Mol. Sci.* **2013**, *3*, 198.
(44) Maier, J. A.; Martinez, C.; Kasavajhala, K.; Wickstrom, L.; Hauser, K. E.; Simmerling, C. *J. Chem. Theory Comput.* **2015**, *11*, 3696.
(45) Ivani, I.; Dans, P. D.; Noy, A.; Pérez, A.; Faustino, I.; Hospital, A.; Walther, J.; Andrio, P.; Goñi, R.; Balaceanu, A.; Portella, G.; Battistini, F.; Gelpí, J. L.; González, C.; Vendruscolo, M.; Laughton, C. A.; Harris, S. A.; Case, D. A.; Orozco, M. *Nat. Methods* **2015**, *13*, 55.
(46) Jorgensen, W. L.; Chandrasekhar, J.; Madura, J. D.; Impey, R. W.; Klein, M. L. *J. Chem. Phys.* **1983**, *79*, 926.
(47) Loncharich, R. J.; Brooks, B. R.; Pastor, R. W. *Biopolymers* **1992**, *32*, 523.
(48) Hardy, D. J.; Wu, Z.; Phillips, J. C.; Stone, J. E.; Skeel, R. D.; Schulten, K. *J. Chem. Theory Comput.* **2015**, *11*, 766.

DOI: 10.1021/jacs.6b11470
J. Am. Chem. Soc. XXXX, XXX, XXX−XXX